JCTC Journal of Chemical Theory and Computation

pubs.acs.org/JCTC Article

Characterizing Conical Intersections of Nucleobases on Quantum Computers

Yuchen Wang, Cameron Cianci, Irma Avdic, Rishab Dutta, Samuel Warren, Brandon Allen, Nam P. Vu, Lea F. Santos, Victor S. Batista, and David A. Mazziotti*

Cite This: J. Chem. Theory Comput. 2025, 21, 1213−1221 Read Online

ACCESS | Metrics & More | Article Recommendations

ABSTRACT: Hybrid quantum-classical computing algorithms offer significant potential for accelerating the calculation of the electronic structure of strongly correlated molecules. In this work, we present the first quantum simulation of conical intersections (CIs) in a biomolecule, cytosine, using a superconducting quantum computer. We apply the contracted quantum eigensolver (CQE)—with comparisons to conventional variational quantum deflation (VQD)—to compute the near-degenerate ground and excited states associated with the conical intersection, a key feature governing the photostability of DNA and RNA. The CQE is based on an exact ansatz for many-electron molecules in the absence of noise—a critically important property for resolving strongly correlated states at CIs. Both methods demonstrate promising accuracy when compared with exact diagonalization, even on noisy intermediate-scale quantum computers, highlighting their potential for advancing the understanding of photochemical and photobiological processes. The ability to simulate these intersections is critical for advancing our knowledge of biological processes like DNA repair and mutation, with potential implications for molecular biology and medical research.

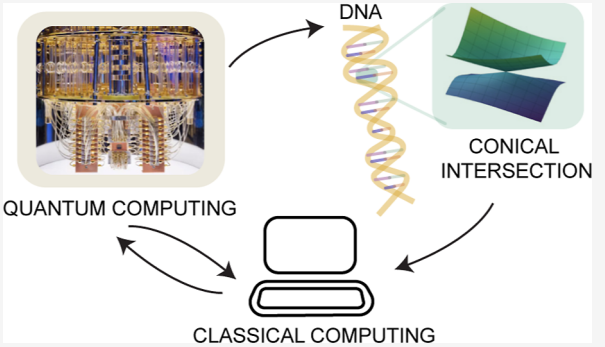

1. INTRODUCTION

Recent advances in quantum computing open new horizons for the field of quantum chemistry with particularly promising applications in electronic structure simulations.[1−4] Various quantum algorithms that demonstrate a potential complexity advantage over classical ones have been proposed. Though still in the noisy intermediate-scale quantum (NISQ) era,[5] electronic structure simulations on quantum devices with appropriate error mitigation are poised to catch up to existing classical methods.[6−12] An apparent application of quantum computing to biology is the electronic structure computation of moderately sized biomolecules.[13,14] For these molecules, most classical wave function-based methods are restricted by a high computational scaling with the number of electrons. While resource-saving methods such as density functional theory can give a reasonable description of excited states,[15,16] they lack the multireference character to describe degenerate electronic states, which are crucial for understanding many photochemical and photobiological processes.

This work explores the nonadiabatic decay of a nucleobase, cytosine, in its photoexcited state. As key components of deoxyribonucleic acid (DNA) and ribonucleic acid (RNA), nucleobases are intrinsically stable when exposed to ultraviolet radiation, preventing the mutations and genetic instability of DNA and RNA, such as those found in many forms of skin cancer.[17] Numerous studies have been conducted on the photobehavior of nucleobases, both from experimental and theoretical perspectives.[18−30] Experimental observations reveal that photoexcited nucleobases exhibit remarkably short lifetimes and low fluorescence yields. These findings suggest that the excited molecules undergo rapid internal conversion, returning to their ground states via conical intersections (CIs) on ultrafast time scales.

CIs are the subspace formed by molecular geometries at which the electronic states are degenerate in energy.[31−37] They are known to be the essential pathway for molecules going through internal conversion, "funneling" the population from excited states to the ground state. The first step toward simulating nonadiabatic molecular dynamics involving multiple electronic states is to characterize the CIs. The degeneracy in energy results in highly multireference character of adiabatic wave functions, which makes single-referenced methods no longer feasible. Additionally, since CIs are seams embedded in

Received: October 24, 2024
Revised: January 11, 2025
Accepted: January 14, 2025
Published: January 28, 2025

the potential energy manifold, they require electronic structure calculations involving batches of molecular geometries, which is a time-consuming task. Quantum computers offer the potential to accelerate electronic structure calculations. Consequently, the development of excited-state quantum algorithms capable of accurately describing CIs on NISQ devices is a critical prerequisite for future research in nonadiabatic molecular dynamics using quantum computing platforms.[38−42]

This study presents to our knowledge the first quantum simulation of CIs in a biomolecule, marking an initial step toward integrating nonadiabatic dynamics into quantum computing platforms and exploring the application of quantum computing in chemical biology. There has been significant effort toward excited state calculations on quantum computers.[43−52] Here, we introduce and test two well-documented quantum algorithms to compute the ground and excited states. The first one is the variational quantum deflation (VQD) and the second one is the contracted quantum eigensolver (CQE). Unlike ref 42 which simulated CIs by computing the ground states for two separate symmetry blocks, these algorithms are designed to compute multiple states within the same symmetry block, suitable for the treatment of accidental CIs.[37] This paper is organized as follows: in the Theory section, we introduce the two quantum algorithms and then provide a brief review of the theory surrounding CIs; in the Results section, we present quantum simulations on noiseless and noisy fake backends, as well as on a 127-qubit IBM quantum computer; finally, we provide conclusions and outlook.

2. THEORY

2.1. Variational Quantum Deflation. The variational quantum deflation (VQD) algorithm is an algorithm to find the k-lowest eigenvalues of a matrix.[45] VQD computes excited states by introducing a deflation term accounting for the orthogonality of eigenvectors. For a system described by the many-electron Schrödinger equation (SE)

$$(\hat{H} - E)|\Psi\rangle = 0 \tag{1}$$

the cost function being optimized takes the following form

$$J(\theta_k) = \langle\Psi(\theta_k)|\hat{H}|\Psi(\theta_k)\rangle + \sum_{j=0}^{k-1} \beta |\langle\Psi(\theta_j)|\Psi(\theta_k)\rangle|^2 \tag{2}$$

in which the k-th wave function is represented by a parametrized ansatz $|\Psi(\theta_k)\rangle$ with parameter set $\{\theta_k\}$ and β is the weight for the nonorthogonal penalty function. The algorithm can be understood as a constrained search that finds the energy minima of the k-th state subject to the constraints that the wave function of the target state must be orthogonal to all $(k - 1)$ lower states. In excited state algorithms, the orthogonality condition is important to prevent the wave function from collapsing into a lower state during optimization. With an appropriate β value, VQD achieves energy minimization while retaining the orthogonality of wave functions, proving to be an efficient and widely used excited state algorithm on NISQ devices.

2.2. Contracted Quantum Eigensolver. The contracted quantum eigensolver (CQE)[10,53−55] is a quantum algorithm originating from the contracted Schrödinger equation (CSE),[56,57] which contracts the SE onto the space of two electrons. Since a molecular Hamiltonian contains up to two-body interaction, the contraction is lossless in the sense that the CSE and the SE share an equivalent set of pure-state solutions.[56,58]

We have introduced two modifications for CQE to tackle excited states. One is by performing variations on an ensemble (subspace) composed of orthogonal pure states[59] and the other is by replacing the Hamiltonian with the variance.[51] The latter is used in this work as it is a state-specific method that can converge to stationary solutions regardless of the energy gap. We first briefly review the method and then provide some comments on different modifications and their performance in characterizing CIs.

The variance of SE is defined as

$$\text{Var} = \langle\Psi|(\hat{H} - E)^2|\Psi\rangle \tag{3}$$

The variance vanishes only when the SE converges to a stationary solution, which in turn allows us to use the nonvanishing residual of the variance to construct an exponential transformation to update the nonstationary wave function.

In variance-based CQE, we minimize the variance at the m-th iteration with respect to the two-body anti-Hermitian operator $\hat{F}_m$

$$\hat{F}_m = \sum_{pqst}{}^2 F_m^{pq;st} \hat{a}_p^\dagger \hat{a}_q^\dagger \hat{a}_t \hat{a}_s \tag{4}$$

and the wave function ansatz is a product of the residuals in eq 3

$$|\Psi_m\rangle = \prod^m e^{\epsilon \hat{F}_m} |\Psi_0\rangle \tag{5}$$

Here $\hat{a}_i^\dagger$ and $\hat{a}_i$ are the creation and annihilation operators with respect to the i-th orbital. The parameter ϵ is the learning rate that can be optimized for better convergence. In each iteration, $\hat{F}$ is evaluated with quantum state tomography. An illustration of the CQE algorithm is given in Figure 1. The algorithm can be characterized as an iterative update of the wave function using a "computed-on-the-fly" residual of the CSE.

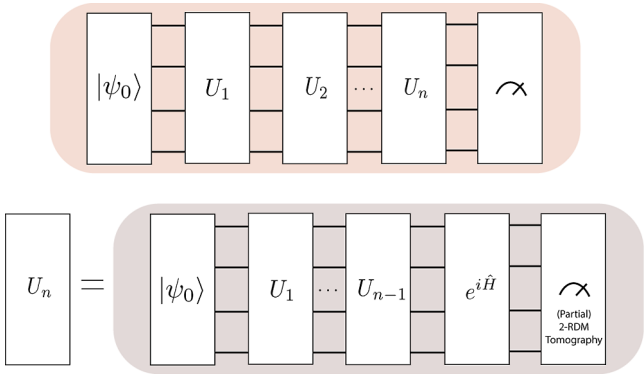

Figure 1. An illustration of the CQE algorithm at the nth iteration.

One difficulty of using the energy variance rather than energy itself is that squaring the Hamiltonian operators typically introduces additional terms that increase the measurement cost. We have used a second-order Taylor expansion to approximate the variance and related variables by preparing an auxiliary state as follows[51]

$$|\tilde{\Psi}_m\rangle = e^{i\delta(\hat{H} - E_m)} |\Psi_m\rangle \tag{6}$$

https://doi.org/10.1021/acs.jctc.4c01434
J. Chem. Theory Comput. 2025, 21, 1213−1221

and then measuring the variance using the following equation

$$\langle\Psi_m|(\hat{H}-E_m)^2|\Psi_m\rangle \approx \frac{1-\Re\langle\Psi_m|\tilde{\Psi}_m\rangle}{\delta^2/2} \tag{7}$$

where the real part of the overlap can be estimated with a Hadamard test procedure,[60] reducing the measurement cost with an ancillary qubit. We present the iterative algorithm of variance-based CQE in Table 1.

Table 1. Variance-Based CQE Algorithm

Algorithm: Variance-based CQE
Given $m = 0$ and convergence tolerance ϵ.
Choose initial wave function $|\Psi_0\rangle$.
Repeat until the energy variance is less than ϵ.
Step 1: Prepare $|\tilde{\Psi}_m\rangle = e^{i\delta(\hat{H}-E_m)}|\Psi_m\rangle$
Step 2: Measure $F_{m+1}^{pq;st}$ and compute $\hat{F}_{m+1}$
Step 3: Prepare $|\Psi_{m+1}\rangle = e^{\epsilon\hat{F}_{m+1}}|\Psi_m\rangle$
Step 4: Optimize variance with respect to ϵ
Step 5: Set $m = m + 1$.

By using the energy variance rather than the energy as the optimization target, the variance-based CQE ensures convergence to local minima, significantly enhancing numerical stability.[51,61] Moreover, it does not require information about lower-energy states, enabling the targeting of specific states during slow-varying changes in molecular geometry. This feature makes the algorithm particularly suitable for describing CIs. The disadvantage of this approach is that orthogonality between wave functions is not guaranteed, which means the target CI state could converge to the other energetically degenerate eigenstate during the optimization process. To address this concern, we use an additional orthogonality check procedure, which involves calculating the overlap between the two converged state vectors. Our simulations did not reveal any instances of such collapsing behavior.

Other popular modifications for calculating the kth excited states, such as the deflation term in VQD and the subspace modification found in SSVQE[46] and parallel CQE,[59] all guarantee the orthogonality of adiabatic wave functions during optimization. However, they require converging all low-lying states either in advance or simultaneously, which can become hard when k is large. Another potential issue is related to the convergence for CIs. At the molecular geometry where energies are exactly degenerate, two eigenvectors can be linearly combined to form new and nonorthogonal eigenvectors.[31] We expect this to slow down the convergence of excited state algorithms based on orthogonality.

2.3. Conical Intersections. In this section, we provide a brief review of key concepts regarding CIs. The diabatic electronic Schrödinger equation is

$$[\mathbf{H^d}(\mathbf{R}) - \mathbf{I}E_J(\mathbf{R})]\mathbf{d}^J(\mathbf{R}) = \mathbf{0} \tag{8}$$

where $\mathbf{H^d}$ is the diabatic Hamiltonian matrix with dimension (N^{state}, N^{state}), and E_J is the energy of the Jth state. While CIs between more than two states are possible, we consider $N^{\text{state}} = 2$ here with the analysis being generalizable. The CIs between two electronic states form only when the two following constraints are simultaneously satisfied

$$H_{11}^d = H_{22}^d,\ H_{12}^d = H_{21}^d = 0 \tag{9}$$

where H_{IJ}^d is the matrix element of $\mathbf{H^d}$. Equation 9 imposed on the global potential energy matrices gives us the $(N-2)$ dimensional seam of CIs. We define the $\mathbf{g}$, $\mathbf{h}$ vectors that lift the branching space[31]

$$\mathbf{g_{12}} = \frac{1}{2}\nabla_{\mathbf{R}}(H_{11}-H_{22}),\quad \mathbf{h_{12}} = \nabla_{\mathbf{R}}H_{12} \tag{10}$$

The $\mathbf{g}$−$\mathbf{h}$ plane is important in understanding nonadiabatic dynamics because the molecules break their degeneracy and achieve a state transition only when moving within the plane, which provides insights on the mode-selective dynamics of nonadiabatic reactions.

The procedure to locate the CI seam and the minimum energy CI (MECI) point in this work is reported in previous literature[40] and a classical implementation can be found in COLUMBUS.[62−64] We use a constrained Lagrangian defined below

$$L(\mathbf{R}) = E_I(\mathbf{R}) + \lambda_0(E_1 - E_2) + \sum_{k=1}^{M}\lambda_k C_k(\mathbf{R}) \tag{11}$$

where C_k are geometric constraints. The Lagrangian is minimized with a Newton−Raphson procedure to find the energy minima subject to energy degeneracy and additional geometry constraints. The gradient needed for the optimization can be obtained on quantum computers with a finite difference method or analytical gradient techniques.[38,65]

3. RESULTS

3.1. Classical Calculation Results. The electronic structure calculations are performed with state-averaged complete active space self-consistent field (SA-CASSCF) in COLUMBUS.[62,63] The first two singlets are averaged with equal weights. We use the correlation-consistent polarized valence double-ζ (cc-pVDZ) basis set and an active space of four electrons in three orbitals. The influence of active space choice on CIs has been extensively investigated in ref 66. Although the active space can significantly affect conical intersection topology, we have to use a relatively small active space in this work due to limitations of current quantum hardware. Therefore, our comparative analysis is deliberately limited to classical results obtained within the same active space. In our analysis, energy levels are considered degenerate if their difference is less than 0.0005 hartree (∼100 cm^{-1}) as determined by exact diagonalization. This level of precision is deemed sufficient given the choice of active space and basis set. The Hamiltonian is constructed from electron integrals in the CASSCF orbital basis. As the Hamiltonian does not guarantee the spin multiplicity (S^2) of the wave function, we perform an additional check to ensure the S^2 values correspond to singlet states.

The CI in cytosine is found along several active vibrational modes—a situation that contributes to the complexity of its rich photochemical behavior. We only investigate the CIs between the first two singlets, which excludes the three-state CIs reported in several previous works.[22−25] There are multiple CIs for the first two singlet states of cytosine.[66] Here we focus on the $\pi\pi^*/S_0$ CI, which has been characterized as the major reaction intermediate for its internal conversion.

Figure 2 reports the minimum energy point on the $\pi\pi^*/S_0$ CIs. That point is optimized classically to an energy difference

https://doi.org/10.1021/acs.jctc.4c01434
J. Chem. Theory Comput. 2025, 21, 1213−1221

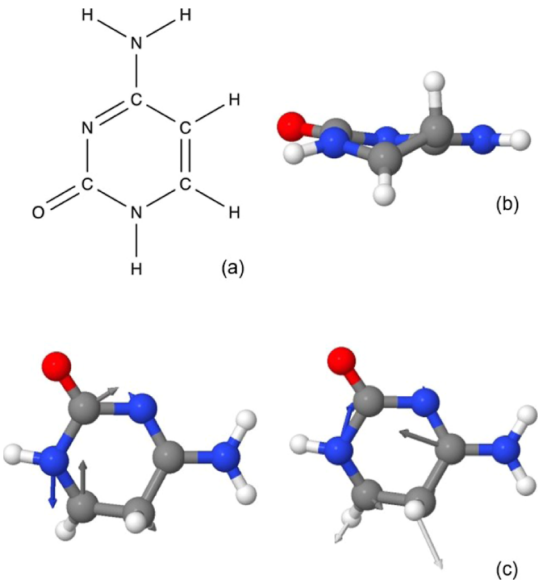

Figure 2. Reported minimum energy CI for cytosine. (a) Chemical structure, (b) planar perspective of the ring structure, (c) the orthogonalized **g** (left), **h** (right) vectors at CI.

between the two CI states of less than 0.0005 and a norm of the constrained Lagrangian in eq 11 of less than 0.01. The CI between $\pi\pi^*$ and S_0 occurs at a distorted molecular structure. The vibrational mode leading to the broken degeneracy is assigned to the out-of-plane torsion (both **g** and **h**) as well as the vibration of the noncoplanar hydrogen (**h**).

3.2. Quantum Simulation Results. While classical calculations capture the electronic structure information of the system within the limits of the employed active space, we now examine the potential applications of quantum computers in characterizing CIs. Two key issues are addressed: first, whether a given quantum algorithm can describe the energy degeneracy and potential energy surface topography in the vicinity of CIs and second, whether CIs can be efficiently optimized with a hybrid method that employs classical optimization and quantum simulation. We have used three different backends in Qiskit[67] in this work:

(i) an ideal statevector simulator without noise, which we use to verify the exactness of the tested algorithms and provide an estimation of the convergence speed in a noiseless environment. For an ideal simulator, the algorithms are not limited by the number of qubits. We thus use the Jordan-Wigner mapping,[68] which is generally a sparse mapping, to map the Hamiltonian to six qubits.

(ii) a fake backend FakeSherbrooke, which we use to mimic the behavior of IBM Sherbrooke.[69] The Fake backend provides a playground for classical optimizers that may require a significant amount of quantum resources. The number of qubits has a significant effect on the quantum algorithm performance in the presence of noise. We employ additional tapering techniques, based on conserving of N (number of electrons) and S_z (total spin number), to reduce the qubits required to four, which is the minimum number of qubits required to avoid truncating the Hamiltonian matrix. An implementation can be found in the ParityMapper in Qiskit.[67]

(iii) The 127-qubit IBM Cleveland with the Eagle r3 type processor,[69] which we use to perform experimental simulations. While IBM Cleveland and Sherbrooke share the same generation of quantum processors, their noise behavior can be quite different.

We report the convergence of both algorithms for a CI Hamiltonian on a noiseless statevector simulator in Figure 3.

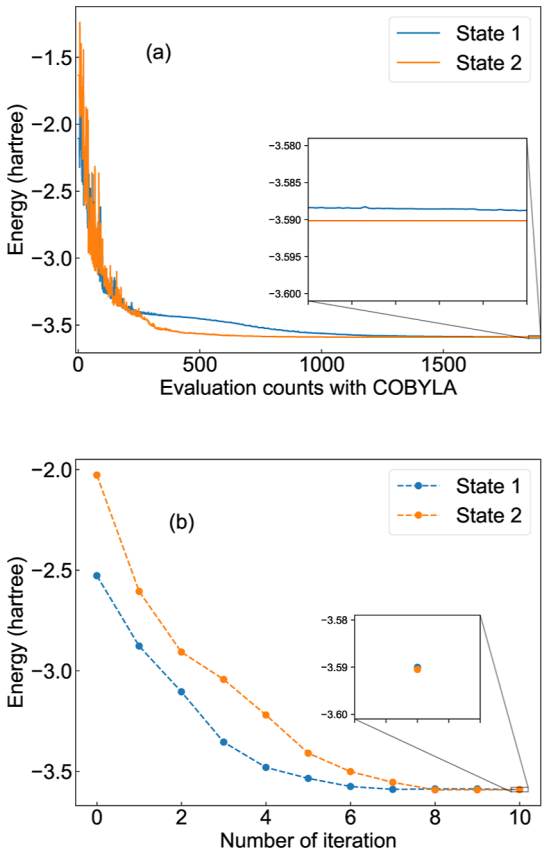

Figure 3. Convergence plot for (a) VQD and (b) CQE on a noiseless simulator. Both ground and first excited singlets are shown. For the energy values on the y axis, the core energy has been excluded from the total energy.

For the VQD calculation, we employ the implementation in Qiskit Algorithm library. A two-local ansatz with four layers is used, which gives a circuit depth of 19. A COBYLA optimizer in Qiskit is used for the classical variation. Figure 3a shows that VQD converges to the threshold with a sufficiently large number of evaluations. The two-local ansatz used here is adequate to parametrize the near-degenerate ground- and excited-state wave functions to the desired accuracy in noiseless simulations. Another observation is that VQD may exhibit state reordering in the vicinity of CIs, where the initial state with lower energy possesses slightly higher energy at convergence. This phenomenon can be rationalized by considering the case of exact degeneracy at CIs, where the VQD cost function exhibits two equivalent global minima that differ only in state ordering. While the algorithm can resolve to the correct ordering as we move to regions sufficiently distant from CIs, the reordering can persist in the vicinity of CIs as a result of the VQD optimization landscape.

CQE has been demonstrated as an exact ansatz[70] and in the noiseless environment we do not restrict the number of

https://doi.org/10.1021/acs.jctc.4c01434
J. Chem. Theory Comput. 2025, 21, 1213−1221

unitaries being applied to verify the exactness. The two states are optimized separately with single Slater determinants as the initial guesses. For the noiseless statevector simulation, it is shown in Figure 3b that CQE converges to the exact solution in fewer than 10 iterations, which is noteworthy given the quantum resources.

We next examine the convergence on the FakeSherbrooke backend. The circuit depth has a significant impact on the algorithm performance in the presence of noise. In order to make a fair comparison, we have restricted the number of iterations and unitaries per iteration of CQE to generate an ansatz with almost the same circuit depth as VQD. We apply 8192 shots to every circuit. The exact value from diagonalization is plotted for comparison. For VQD and CQE, the absolute errors without any error mitigation techniques are ∼60 and ∼40 mhartree, respectively, which is a consequence of the quantum noise. While the absolute error could be improved with error mitigation techniques, we here focus only on the description of the energy gap from the unmitigated results. As can be seen from Figure 4, the error of

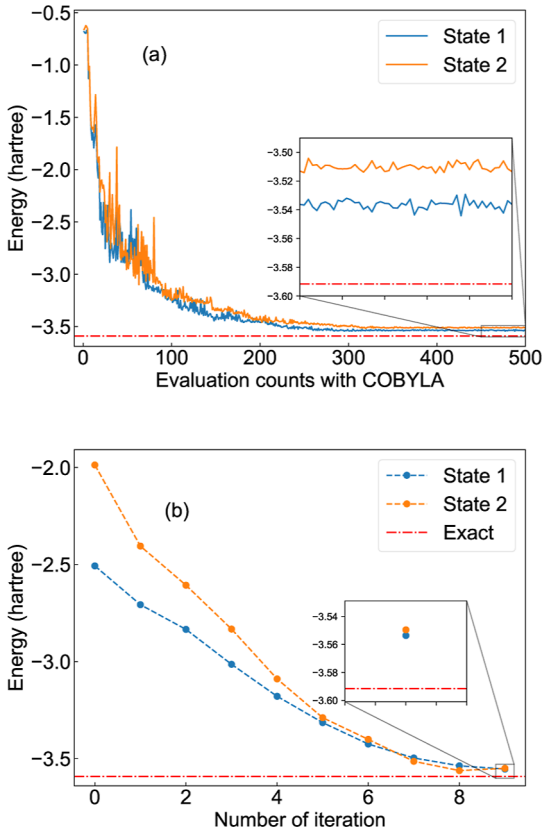

Figure 4. Convergence plot for (a) VQD and (b) CQE on FakeSherbrooke. Both ground and first excited singlets are shown. For the energy values on the *y* axis, the core energy has been excluded from the total energy.

the energy gap is only ∼20 mhartree for VQD and single-digit mhartree at the ninth iteration of CQE. In both methods the energy gap exhibits a smaller error than the absolute energies due to error cancellation.

We observe that CQE outperforms VQD in characterizing the CIs. One reason, discussed in the Theory section, is that the variance-based CQE is a state-specific method, while VQD is dependent upon the given state and any energetically equal or lower states, which can slow the convergence for near-degenerate states. Another possible reason is that the CQE uses the ansatz from the ACSE,[71,72] which is a physics-informed exact ansatz, while the VQD, implemented in this work, employs a two-local ansatz that does not account for the structure of the Hamiltonian or other physical insights into the system. A more efficient ansatz, such as the unitary coupled cluster[73,74] or the ACSE ansatz,[55,71,72] is advised for VQD to achieve better performance.

One may also draw a rough comparison between the quantum resources. It takes around 320 evaluations for VQD to converge with the COBYLA optimizer, while it takes eight iterations for CQE. We note that for each iteration, CQE requires a two-particle reduced density matrix (2-RDM) tomography, leading to a similar number of total measurements comparing to VQD. However, quantum state tomography can be implemented in a highly parallel way by simultaneously preparing and measuring multiple copies of the target quantum state while in VQD, the iterations are usually much longer. Moreover, because the CQE exploits the restriction to pairwise interactions in the Hamiltonian, the CQE for any number N of electrons depends only on the 2-RDM, which has a scaling of $O(r^4)$ with orbital number r (with tomography protocol even less[75]), making it a good candidate for scalable molecular simulations with large active spaces.

After the fake backend experiments, we use the CQE to characterize the topography of the CI on a real IBM quantum computer. Several error mitigation techniques are used to suppress the error on IBM Cleveland, which are described in detail in the Supporting Information of ref 76. We utilize Qiskit's built-in zero noise extrapolation, gate twirling and Twirled Readout Error eXtinction (TREX) for error mitigation.[67] Moreover, in the CQE we have applied a dynamical threshold to the unitaries[10] in which after decomposing the unitaries in the Pauli basis, we select only those with coefficients above a threshold that decreases dynamically with convergence.

We span the grid of molecular geometry along the **g**, **h** directions and plot the coupled 3D potential energy surfaces in the vicinity of the CI. The exact surface and the surface from quantum simulation are shown in Figure 5a,b, respectively. The surfaces from real quantum computers deviate slightly from the exact surfaces in absolute energies, and they are not as smooth as the exact ones. However, the topography of the double cone is generally well-preserved. The degenerate point in Figure 5a is no longer degenerate in Figure 5b due to noise, but the two points are not far away. As has been observed in single-point calculations, if the error generated from quantum noise is uniform, then the only effect of noise is to shift the absolute value of the upper and lower surfaces by a certain amount, which in principle should not affect the nonadiabatic dynamics significantly. The ability to characterize the electronic structure of the strongly correlated states at CIs provides an important step toward practical applications for the simulation of nonadiabatic dynamics on NISQ devices.

We further can locate CIs with a hybrid quantum-classical optimization method to minimize the energy gap as a function of the nuclear coordinates. Here we obtained numerical nuclear gradients by performing finite differences in Cartesian coordinates. The stepsize employed is 0.01. For the ease of implementation, we only allow the coordinate of the hydrogen atom with the greatest vibrational amplitude in the **g**−**h** plane to vary while keeping the rest of the molecule fixed. The

https://doi.org/10.1021/acs.jctc.4c01434
J. Chem. Theory Comput. 2025, 21, 1213−1221

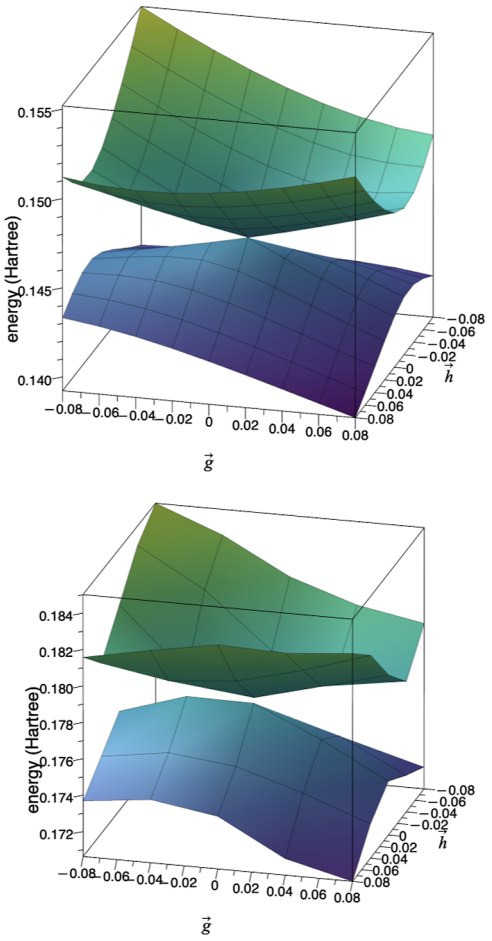

Figure 5. 3D CI topography shown with (a) exact diagonalization (b) quantum simulation with IBM Cleveland. The energies in z axis are the relative values compared to global minima of −392.6536. The grid size is (9,9) for (a) and (5,5) for (b).

optimization results are provided in Table 2. At each iteration, we report the quantum simulation and exact diagonalization results at the same molecular geometry. The energy gap decreases at every iteration with the energy gap's error being well below the absolute error of individual states. We are able to converge the geometry optimization within single mhartree accuracy, which is noteworthy given the noisy nature of current quantum computers. We also observe that the energy difference during optimization can be quite stochastic (e.g., between iterations 3 and 4) even though we only have three degrees of freedom. The reason for this behavior is that in the presence of noise, the nuclear gradients obtained from finite differences may be subject to large deviations. A stochastic optimizer such as Simultaneous Perturbation Stochastic Approximation[77] may provide better convergence when the quantum resources are limited and the number of nuclear degrees of freedom is larger.

4. CONCLUSIONS

In this work we simulate the electronic structure of the ground and excited states of cytosine with quantum computers, focusing on the conical intersection—the crucial region for nonadiabatic dynamics simulations. We examine two quantum algorithms for excited state calculations: variational quantum deflation (VQD) and contracted quantum eigensolver (CQE), for performing crucial tasks for nonadiabatic dynamics such as the calculation of near-degenerate energies and the optimization of CI geometries. The CQE displays slightly better performance with cytosine due to its state-specific modification and the physics-informed ansatz. For larger molecules and active spaces, the CQE would outperform the two-local VQD and other nonphysics-based ansatzes. Moreover, the CQE is based on the CSE ansatz—an exact ansatz for many-electron molecules in the absence of noise—, which is critical for resolving strongly correlated states such as those involved in the conical intersection.

Electronic structure methods that accurately describe CIs are essential for nonadiabatic dynamics, reaction path finding and chemical kinetic modeling. CQE as a nonvariational quantum algorithm, demonstrates benefits including: (1) shallow ansatz depth through on-the-fly thresholding of the residual; (2) scalable tomography cost;[76] (3) ability to reproduce qualitatively correct topography of CIs in the presence of noise. Future work will examine the use of the CQE algorithm within nonadiabatic dynamic simulations. The present work represents an important first step toward harnessing the potential of quantum computers to provide more accurate and efficient descriptions of conical interactions for accelerated progress in both photochemistry and photobiology.

AUTHOR INFORMATION

Corresponding Author

David A. Mazziotti − *Department of Chemistry and The James Franck Institute, The University of Chicago, Chicago, Illinois 60637, United States;* orcid.org/0000-0002-9938-3886; Email: damazz@uchicago.edu

Authors

Yuchen Wang − *Department of Chemistry and The James Franck Institute, The University of Chicago, Chicago, Illinois 60637, United States;* orcid.org/0000-0003-0479-3776

Cameron Cianci − *Department of Physics, University of Connecticut, Storrs, Connecticut 06269, United States;*

Table 2. Optimization Process for CIs on Quantum Computers[a]

iteration	E_0 (simulation)	E_1 (simulation)	ΔE (simulation)	E_0 (exact)	E_1 (exact)	ΔE (exact)
0	0.1620	0.2313	0.0693	0.1401	0.2081	0.0680
1	0.1714	0.2229	0.0515	0.1408	0.1964	0.0556
2	0.1812	0.2112	0.0300	0.1416	0.1843	0.0427
3	0.1897	0.2036	0.0139	0.1430	0.1684	0.0254
4	0.1770	0.1959	0.0189	0.1436	0.1618	0.0182
5	0.1762	0.1841	0.0079	0.1449	0.1551	0.0102

[a]Energies are reported with respect to the global minima of −392.6536. Unit is hartree.

https://doi.org/10.1021/acs.jctc.4c01434
J. Chem. Theory Comput. 2025, 21, 1213−1221

Mirion Technologies (Canberra) Inc., Meriden, Connecticut 06450, United States

Irma Avdic − *Department of Chemistry and The James Franck Institute, The University of Chicago, Chicago, Illinois 60637, United States;* orcid.org/0000-0002-0731-9693

Rishab Dutta − *Department of Chemistry, Yale University, New Haven, Connecticut 06520-8107, United States;* orcid.org/0000-0001-7675-1431

Samuel Warren − *Department of Chemistry and The James Franck Institute, The University of Chicago, Chicago, Illinois 60637, United States*

Brandon Allen − *Department of Chemistry, Yale University, New Haven, Connecticut 06520-8107, United States;* orcid.org/0000-0002-5512-1892

Nam P. Vu − *Department of Chemistry, Yale University, New Haven, Connecticut 06520-8107, United States; Department of Chemistry, Lafayette College, Easton, Pennsylvania 18042, United States;* orcid.org/0000-0002-3849-5139

Lea F. Santos − *Department of Physics, University of Connecticut, Storrs, Connecticut 06269, United States*

Victor S. Batista − *Department of Chemistry, Yale University, New Haven, Connecticut 06520-8107, United States;* orcid.org/0000-0002-3262-1237

Complete contact information is available at: https://pubs.acs.org/10.1021/acs.jctc.4c01434

Notes

The authors declare no competing financial interest.

■ ACKNOWLEDGMENTS

D.A.M. gratefully acknowledges the U.S. National Science Foundation Grant no. CHE-2155082 and the U.S. Department of Energy, Office of Basic Energy Sciences, grant DE-SC0019215. I.A. gratefully acknowledges the NSF Graduate Research Fellowship Program under Grant no. 2140001. V.S.B. and L.F.S. acknowledge support from the National Science Foundation Engines Development Award: Advancing Quantum Technologies (CT) under Award Number 2302908, and partial support from the National Science Foundation Center for Quantum Dynamics on Modular Quantum Devices (CQD-MQD) under Award Number 2124511. The views expressed are those of the authors and do not reflect the official policy or position of IBM or the IBMQ team.

■ REFERENCES

(1) Aspuru-Guzik, A.; Dutoi, A. D.; Love, P. J.; Head-Gordon, M. Simulated quantum computation of molecular energies. *Science* **2005**, *309*, 1704.

(2) Cao, Y.; Romero, J.; Olson, J. P.; Degroote, M.; Johnson, P. D.; Kieferová, M.; Kivlichan, I. D.; Menke, T.; Peropadre, B.; Sawaya, N. P.; et al. Quantum chemistry in the age of quantum computing. *Chem. Rev.* **2019**, *119*, 10856.

(3) Bauer, B.; Bravyi, S.; Motta, M.; Chan, G. K.-L. Quantum algorithms for quantum chemistry and quantum materials science. *Chem. Rev.* **2020**, *120*, 12685.

(4) Dutta, R.; Cabral, D. G.; Lyu, N.; Vu, N. P.; Wang, Y.; Allen, B.; Dan, X.; Cortiñas, R. G.; Khazaei, P.; Smart, S. E.; et al. Simulating chemistry on bosonic quantum devices. *arXiv* **2024**, arXiv:2404.10214.

(5) Preskill, J. Quantum computing in the nisq era and beyond. *Quantum* **2018**, *2*, 79.

(6) Kandala, A.; Mezzacapo, A.; Temme, K.; Takita, M.; Brink, M.; Chow, J. M.; Gambetta, J. M. Hardware-efficient variational quantum eigensolver for small molecules and quantum magnets. *Nature* **2017**, *549*, 242.

(7) Russo, A. E.; Rudinger, K. M.; Morrison, B. C.; Baczewski, A. D. Evaluating energy differences on a quantum computer with robust phase estimation. *Phys. Rev. Lett.* **2021**, *126*, 210501.

(8) Tang, H. L.; Shkolnikov, V.; Barron, G. S.; Grimsley, H. R.; Mayhall, N. J.; Barnes, E.; Economou, S. E. qubit-adapt-vqe: An adaptive algorithm for constructing hardware-efficient ansätze on a quantum processor. *PRX Quantum* **2021**, *2*, 020310.

(9) Sureshbabu, S. H.; Sajjan, M.; Oh, S.; Kais, S. Implementation of quantum machine learning for electronic structure calculations of periodic systems on quantum computing devices. *J. Chem. Inf. Model.* **2021**, *61*, 2667.

(10) Smart, S. E.; Boyn, J.-N.; Mazziotti, D. A. Resolving correlated states of benzyne with an error-mitigated contracted quantum eigensolver. *Phys. Rev. A* **2022**, *105*, 022405.

(11) Dutta, R.; Vu, N. P.; Lyu, N.; Wang, C.; Batista, V. S. Simulating electronic structure on bosonic quantum computers. *arXiv* **2024**, arXiv:2404.10222.

(12) Cianci, C.; Santos, L. F.; Batista, V. S. Subspace-search quantum imaginary time evolution for excited state computations. *arXiv* **2024**, arXiv:2407.11182.

(13) Cao, Y.; Romero, J.; Aspuru-Guzik, A. Potential of quantum computing for drug discovery. *IBM J. Res. Dev.* **2018**, *62* (6), 6.

(14) Smaldone, A. M.; Batista, V. S. Quantum-to-classical neural network transfer learning applied to drug toxicity prediction. *J. Chem. Theory Comput.* **2024**, *20*, 4901−4908.

(15) Varsano, D.; Di Felice, R.; Marques, M. A.; Rubio, A. A TDDFT study of the excited states of DNA bases and their assemblies. *J. Phys. Chem. B* **2006**, *110*, 7129.

(16) Teh, H.-H.; Subotnik, J. E. The simplest possible approach for simulating S_0−S_1 conical intersections with DFT/TDDFT: Adding one doubly excited configuration. *J. Phys. Chem. Lett.* **2019**, *10*, 3426.

(17) Marrot, L.; Meunier, J.-R. Skin dna photodamage and its biological consequences. *J. Am. Acad. Dermatol.* **2008**, *58*, S139.

(18) Kang, H.; Lee, K. T.; Jung, B.; Ko, Y. J.; Kim, S. K. Intrinsic lifetimes of the excited state of DNA and RNA bases. *J. Am. Chem. Soc.* **2002**, *124*, 12958.

(19) Malone, R. J.; Miller, A. M.; Kohler, B. Singlet Excited-state Lifetimes of Cytosine Derivatives Measured by Femtosecond Transient Absorption¶. *Photochem. Photobiol.* **2007**, *77*, 158−164.

(20) Sharonov, A.; Gustavsson, T.; Carré, V.; Renault, E.; Markovitsi, D. Cytosine excited state dynamics studied by femtosecond fluorescence upconversion and transient absorption spectroscopy. *Chem. Phys. Lett.* **2003**, *380*, 173.

(21) Merchán, M.; Serrano-Andrés, L. Ultrafast internal conversion of excited cytosine via the lowest $\pi\pi^*$ electronic singlet state. *J. Am. Chem. Soc.* **2003**, *125*, 8108.

(22) Blancafort, L.; Robb, M. A. Key role of a threefold state crossing in the ultrafast decay of electronically excited cytosine. *J. Phys. Chem. A* **2004**, *108*, 10609.

(23) Matsika, S. Three-state conical intersections in nucleic acid bases. *J. Phys. Chem. A* **2005**, *109*, 7538.

(24) Kistler, K. A.; Matsika, S. Three-state conical intersections in cytosine and pyrimidinone bases. *J. Chem. Phys.* **2008**, *128*, 215102.

(25) González-Vázquez, J.; González, L. A time-dependent picture of the ultrafast deactivation of keto-cytosine including three-state conical intersections. *ChemPhysChem* **2010**, *11*, 3617.

(26) Barbatti, M.; Aquino, A. J.; Szymczak, J. J.; Nachtigallova, D.; Lischka, H. Photodynamical simulations of cytosine: characterization of the ultrafast bi-exponential uv deactivation. *Phys. Chem. Chem. Phys.* **2011**, *13*, 6145.

(27) Richter, M.; Marquetand, P.; Gonzalez-Vazquez, J.; Sola, I.; González, L. Femtosecond intersystem crossing in the DNA nucleobase cytosine. *J. Phys. Chem. Lett.* **2012**, *3*, 3090.

(28) Blaser, S.; Trachsel, M. A.; Lobsiger, S.; Wiedmer, T.; Frey, H.-M.; Leutwyler, S. Gas-phase cytosine and cytosine-n1-derivatives have 0.1−1 ns lifetimes near the s1 state minimum. *J. Phys. Chem. Lett.* **2016**, *7*, 752.

(29) Trachsel, M. A.; Blaser, S.; Lobsiger, S.; Siffert, L.; Frey, H.-M.; Blancafort, L.; Leutwyler, S. Locating cytosine conical intersections by laser experiments and ab initio calculations. *J. Phys. Chem. Lett.* **2020**, *11*, 3203.
(30) Shahrokh, L.; Omidyan, R.; Azimi, G. Theoretical insights on the excited-state-deactivation mechanisms of protonated thymine and cytosine. *Phys. Chem. Chem. Phys.* **2021**, *23*, 8916.
(31) Yarkony, D. R. Diabolical conical intersections. *Rev. Mod. Phys.* **1996**, *68*, 985.
(32) Domcke, W.; Yarkony, D.; Köppel, H. *Conical Intersections: Electronic Structure, Dynamics & Spectroscopy*; World Scientific, 2004; Vol. *15*.
(33) Levine, B. G.; Martínez, T. J. Isomerization through conical intersections. *Annu. Rev. Phys. Chem.* **2007**, *58*, 613.
(34) Matsika, S.; Krause, P. Nonadiabatic events and conical intersections. *Annu. Rev. Phys. Chem.* **2011**, *62*, 621.
(35) Tully, J. C. Perspective: Nonadiabatic dynamics theory. *J. Chem. Phys.* **2012**, *137*, 22A301.
(36) Guo, H.; Yarkony, D. R. Accurate nonadiabatic dynamics. *Phys. Chem. Chem. Phys.* **2016**, *18*, 26335.
(37) Yarkony, D. R.; Xie, C.; Zhu, X.; Wang, Y.; Malbon, C. L.; Guo, H. Diabatic and adiabatic representations: Electronic structure caveats. *Comput. Theor. Chem.* **2019**, *1152*, 41.
(38) Yalouz, S.; Senjean, B.; Günther, J.; Buda, F.; O'Brien, T. E.; Visscher, L. A state-averaged orbital-optimized hybrid quantum−classical algorithm for a democratic description of ground and excited states. *Quantum Sci. Technol.* **2021**, *6*, 024004.
(39) Ollitrault, P. J.; Mazzola, G.; Tavernelli, I. Nonadiabatic molecular quantum dynamics with quantum computers. *Phys. Rev. Lett.* **2020**, *125*, 260511.
(40) Wang, Y.; Mazziotti, D. A. Quantum simulation of conical intersections. *Phys. Chem. Chem. Phys.* **2024**, *26*, 11491.
(41) Koridon, E.; Fraxanet, J.; Dauphin, A.; Visscher, L.; O'Brien, T. E.; Polla, S. A hybrid quantum algorithm to detect conical intersections. *Quantum* **2024**, *8*, 1259.
(42) Zhao, S.; Tang, D.; Xiao, X.; Wang, R.; Sun, Q.; Chen, Z.; Cai, X.; Li, Z.; Yu, H.; Fang, W.-H. Quantum computation of conical intersections on a programmable superconducting quantum processor. *J. Phys. Chem. Lett.* **2024**, *15*, 7244−7253.
(43) McClean, J. R.; Kimchi-Schwartz, M. E.; Carter, J.; De Jong, W. A. Hybrid quantum-classical hierarchy for mitigation of decoherence and determination of excited states. *Phys. Rev. A* **2017**, *95*, 042308.
(44) Colless, J. I.; Ramasesh, V. V.; Dahlen, D.; Blok, M. S.; Kimchi-Schwartz, M. E.; McClean, J. R.; Carter, J.; de Jong, W. A.; Siddiqi, I. Computation of molecular spectra on a quantum processor with an error-resilient algorithm. *Phys. Rev. X* **2018**, *8*, 011021.
(45) Higgott, O.; Wang, D.; Brierley, S. Variational quantum computation of excited states. *Quantum* **2019**, *3*, 156.
(46) Nakanishi, K. M.; Mitarai, K.; Fujii, K. Subspace-search variational quantum eigensolver for excited states. *Phys. Rev. Res.* **2019**, *1*, 033062.
(47) Ollitrault, P. J.; Kandala, A.; Chen, C.-F.; Barkoutsos, P. K.; Mezzacapo, A.; Pistoia, M.; Sheldon, S.; Woerner, S.; Gambetta, J. M.; Tavernelli, I. Quantum equation of motion for computing molecular excitation energies on a noisy quantum processor. *Phys. Rev. Res.* **2020**, *2*, 043140.
(48) Asthana, A.; Kumar, A.; Abraham, V.; Grimsley, H.; Zhang, Y.; Cincio, L.; Tretiak, S.; Dub, P. A.; Economou, S. E.; Barnes, E.; et al. Quantum self-consistent equation-of-motion method for computing molecular excitation energies, ionization potentials, and electron affinities on a quantum computer. *Chem. Sci.* **2023**, *14*, 2405.
(49) Kumar, A.; Asthana, A.; Abraham, V.; Crawford, T. D.; Mayhall, N. J.; Zhang, Y.; Cincio, L.; Tretiak, S.; Dub, P. A. Quantum simulation of molecular response properties in the nisq era. *J. Chem. Theory Comput.* **2023**, *19*, 9136.
(50) Kim, Y.; Krylov, A. I. Two algorithms for excited-state quantum solvers: Theory and application to eom-uccsd. *J. Phys. Chem. A* **2023**, *127*, 6552.
(51) Wang, Y.; Mazziotti, D. A. Electronic excited states from a variance-based contracted quantum eigensolver. *Phys. Rev. A* **2023**, *108*, 022814.
(52) Ding, L.; Hong, C.-L.; Schilling, C. Ground and Excited States from Ensemble Variational Principles. *Quantum* **2024**, *8*, 1525.
(53) Smart, S. E.; Mazziotti, D. A. Quantum solver of contracted eigenvalue equations for scalable molecular simulations on quantum computing devices. *Phys. Rev. Lett.* **2021**, *126*, 070504.
(54) Wang, Y.; Sager-Smith, L. M.; Mazziotti, D. A. Quantum simulation of bosons with the contracted quantum eigensolver. *New J. Phys.* **2023**, *25*, 103005.
(55) Warren, S.; Wang, Y.; Benavides-Riveros, C. L.; Mazziotti, D. A. Exact ansatz of fermion-boson systems for a quantum device. *Phys. Rev. Lett.* **2024**, *133*, 080202.
(56) Mazziotti, D. A. Contracted Schrödinger equation: Determining quantum energies and two-particle density matrices without wave functions. *Phys. Rev. A:At., Mol., Opt. Phys.* **1998**, *57*, 4219.
(57) Mazziotti, D. A. Anti-hermitian contracted Schrödinger equation: Direct determination of the two-electron reduced density matrices of many-electron molecules. *Phys. Rev. Lett.* **2006**, *97*, 143002.
(58) Nakatsuji, H. Equation for the direct determination of the density matrix. *Phys. Rev. A:At., Mol., Opt. Phys.* **1976**, *14*, 41.
(59) Benavides-Riveros, C. L.; Wang, Y.; Warren, S.; Mazziotti, D. A. Quantum simulation of excited states from parallel contracted quantum eigensolvers. *New J. Phys.* **2024**, *26*, 033020.
(60) Cleve, R.; Ekert, A.; Macchiavello, C.; Mosca, M. Quantum algorithms revisited. *Proc. R. Soc. London, Ser. A* **1998**, *454*, 339.
(61) Alcoba, D. R.; Lain, L.; Torre, A.; Ayala, T. R.; Oña, O. B.; Massaccesi, G. E.; Peralta, J. E.; Melo, J. I. Generalized spin in the variance-based wave function optimization method within the doubly occupied configuration interaction framework. *J. Phys. Chem. A* **2024**, *128*, 7277.
(62) Lischka, H.; Müller, T.; Szalay, P. G.; Shavitt, I.; Pitzer, R. M.; Shepard, R. Columbus-a program system for advanced multireference theory calculations. *Wiley Interdiscip. Rev.:Comput. Mol. Sci.* **2011**, *1*, 191.
(63) Lischka, H.; Shepard, R.; Müller, T.; Szalay, P. G.; Pitzer, R. M.; Aquino, A. J.; Araújo do Nascimento, M. M.; Barbatti, M.; Belcher, L. T.; Blaudeau, J.-P.; et al. The generality of the guga mrci approach in columbus for treating complex quantum chemistry. *J. Chem. Phys.* **2020**, *152*, 134110.
(64) Manaa, M. R.; Yarkony, D. R. On the intersection of two potential energy surfaces of the same symmetry. systematic characterization using a lagrange multiplier constrained procedure. *J. Chem. Phys.* **1993**, *99*, 5251.
(65) Yalouz, S.; Koridon, E.; Senjean, B.; Lasorne, B.; Buda, F.; Visscher, L. Analytical nonadiabatic couplings and gradients within the state-averaged orbital-optimized variational quantum eigensolver. *J. Chem. Theory Comput.* **2022**, *18*, 776.
(66) Cuéllar-Zuquin, J.; Pepino, A. J.; Fdez Galván, I.; Rivalta, I.; Aquilante, F.; Garavelli, M.; Lindh, R.; Segarra-Martí, J. Characterizing Conical Intersections in DNA/RNA Nucleobases with Multiconfigurational Wave Functions of Varying Active Space Size. *J. Chem. Theory Comput.* **2023**, *19*, 8258−8272.
(67) Qiskit Research Community *Qiskit: An Open-Source Framework for Quantum Computing*, 2024.
(68) Jordan, P.; Wigner, E. Über das paulische Äquivalenzverbot. *Z. Phys.* **1928**, *47*, 631−651.
(69) IBM-Quantum, https://quantum-computing.ibm.com/, 2024.
(70) Smart, S. E.; Mazziotti, D. A. Verifiably exact solution of the electronic schrödinger equation on quantum devices. *Phys. Rev. A* **2024**, *109*, 022802.
(71) Mazziotti, D. A. Anti-Hermitian part of the contracted Schrödinger equation for the direct calculation of two-electron reduced density matrices. *Phys. Rev. A:At., Mol., Opt. Phys.* **2007**, *75*, 022505.

(72) Mazziotti, D. A. Exactness of wave functions from two-body exponential transformations in many-body quantum theory. *Phys. Rev. A:At., Mol., Opt. Phys.* **2004**, *69*, 012507.
(73) Hoffmann, M. R.; Simons, J. A unitary multiconfigurational coupled-cluster method: Theory and applications. *J. Chem. Phys.* **1988**, *88*, 993−1002.
(74) Romero, J.; Babbush, R.; McClean, J. R.; Hempel, C.; Love, P. J.; Aspuru-Guzik, A. Strategies for quantum computing molecular energies using the unitary coupled cluster ansatz. *Quantum Sci. Technol.* **2019**, *4*, 014008.
(75) Bonet-Monroig, X.; Babbush, R.; O'Brien, T. E. Nearly optimal measurement scheduling for partial tomography of quantum states. *Phys. Rev. X* **2020**, *10*, 031064.
(76) Wang, Y.; Avdic, I.; Mazziotti, D. A. Shadow ansatz for the many-fermion wave function in scalable molecular simulations on quantum computing devices. *arXiv* **2024**, arXiv:2408.11026.
(77) Spall, J. C. Implementation of the simultaneous perturbation algorithm for stochastic optimization. *IEEE Trans. Aerosp. Electron. Syst.* **1998**, *34*, 817.

https://doi.org/10.1021/acs.jctc.4c01434
J. Chem. Theory Comput. 2025, 21, 1213−1221